

SUPPLEMENTARY INFORMATION

Self assembled monolayer of silica nanoparticles with improved order by drop casting

Authors:

Asma Qdemat^{1,2}, Emmanuel Kentzinger¹, Johan Buitenhuis³,
Ulrich Rücker¹, Marina Ganeva⁴, Thomas Brückel^{1,2}

Affiliations:

¹Jülich Centre for Neutron Science and Peter Grünberg Institute,
JARA-FIT, Forschungszentrum Jülich GmbH, 52425 Jülich,
Germany

²RWTH Aachen, Lehrstuhl für Experimentalphysik IVc, Jülich-Aachen
Research Alliance (JARA-FIT), 52074 Aachen, Germany.

³Biomacromolecular Systems and Processes, IBI-4, Forschungszentrum
Jülich GmbH, 52425 Jülich, Germany.

⁴ Forschungszentrum Jülich GmbH, Jülich Center for Neutron
Science at MLZ Lichtenberg street, 85748 Garching, Germany

1 NPs characterization

The structural properties of the monodispersed spherical SiO₂ NPs have been investigated by several methods. The nanoparticles were analyzed by small-angle X-ray scattering (SAXS) using the GALAXI instrument at FZJ, Jülich, Germany, in order to obtain the particle size and the size distribution. The SAXS result of the NPs dispersion with a concentration of 5.4% is shown in Fig.1 (a). Fitting of the SAXS data assuming a spherical form factor yields an average NP diameter of 49 ± 0.4 nm with a size distribution of 2.8%. In addition, the particles were analyzed by SEM using a Hitachi SU8000 microscope. Fig.1 (b) shows an SEM image of the NPs obtained

Table 1: Particle size and size distribution as determined from TEM, SEM, SAXS, DLS of stearyl silica particles.

parameters	SEM	TEM	SAXS	DLS
2R (nm)	48.8 ± 1.5	51.4 ± 0.8	49 ± 0.4	55.2 ± 1.6
σ (%)	3	6	2.8	-

after deposition of 5 μL of nanoparticles dispersion with a concentration of 5.4 vol% on the silicon substrate by drop-casting and the solvent was allowed to evaporate rapidly. SEM clearly reveals that the particles are regular spherical particles. Once deposited on a silicon wafer, they tend to self-organize in a regular hexagonal layer without agglomeration. The inset in Fig.1 (b) shows the size distribution of the particles with a lognormal fit according to Fig. 1 (b) obtained from a statistical analysis of 100 particles. The fitting yields a mean particle diameter of 48.8 ± 1.5 nm with a size distribution of 3%. TEM yields a mean diameter of 51.4 nm by measuring several rows with 10 particles, which should include the thickness of the dry (collapsed) stearyl layer. Furthermore, dynamic light scattering (DLS) was used for the NPs characterization, which yields a mean diameter of 55.2 nm. This is larger than the values obtained from the other techniques because DLS measures the hydrodynamic radius, which means the core radius with the stearyl alcohol molecule around it, whereas SAXS only measures the core size.

2 Formation of NP monolayers and local characterization by SEM

2.1 Method 1: Nanoparticles monolayer by simple drop casting

Fig. 2 shows SEM image of the SiO_2 NP monolayers obtained by Method 1: simple drop casting without adding additional toluene and reducing its evaporation rate by covering the sample as described in the experimental section in the main text. From the

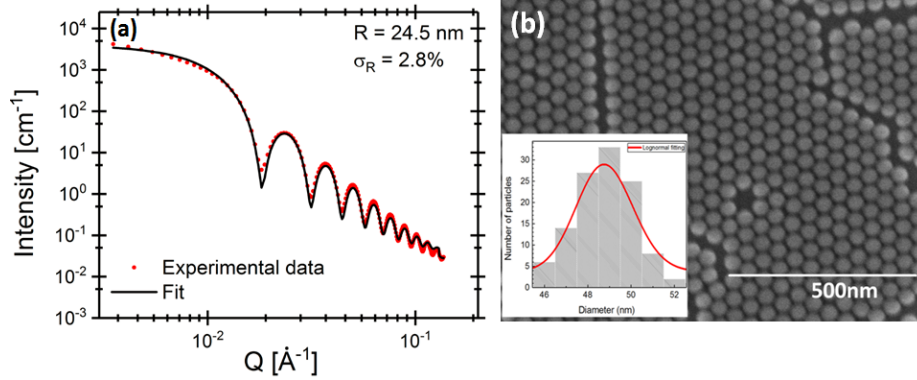


Figure 1: (a) SAXS pattern of SiO_2 NPs stock dispersion together with the fit (black line) to the data (red circles) assuming a spherical form factor and, (b) SEM image of SiO_2 NPs. The inset shows the size distribution along with a lognormal fit (red line).

image, it is seen that the results observed are the same as the results observed of the SiO_2 NP monolayers obtained with adding additional toluene (Fig.1 in the main text).

3 Structural characterization of NP arrangement on silicon surface

3.1 X-ray reflectivity

To fit the measured XRR curve of the monolayers obtained after 10 days of heat treatment shown in Fig. 4 (c) in the main text, we assumed the layer model drawn in Fig. 4 (d) consisting of the particle layer on top of the silicon substrate (dark gray). The left side shows the cross-section of the model and the right side shows the expected scattering length density depth profile for the particle layer with ideal spherical particles.

The average SLD within the nanoparticles layer given as $\rho(Z) = \rho_1 - \rho_2 \left(\frac{Z-R}{R}\right)^2$ has a parabolic line shape with the maximum value $\rho_1 = 16.7(1) \times 10^{-6} \text{ \AA}^{-2}$ in the center of the nanoparticle layer set at $Z = R$. The average SLD value at $Z = 0$ and $Z = 2R = \rho_1 - \rho_2 = 16.7 - 12.7 = 4(1) \times 10^{-6} \text{ \AA}^{-2}$ where R is the spherical radius and $2R = D$ is the thickness of the nanoparticles

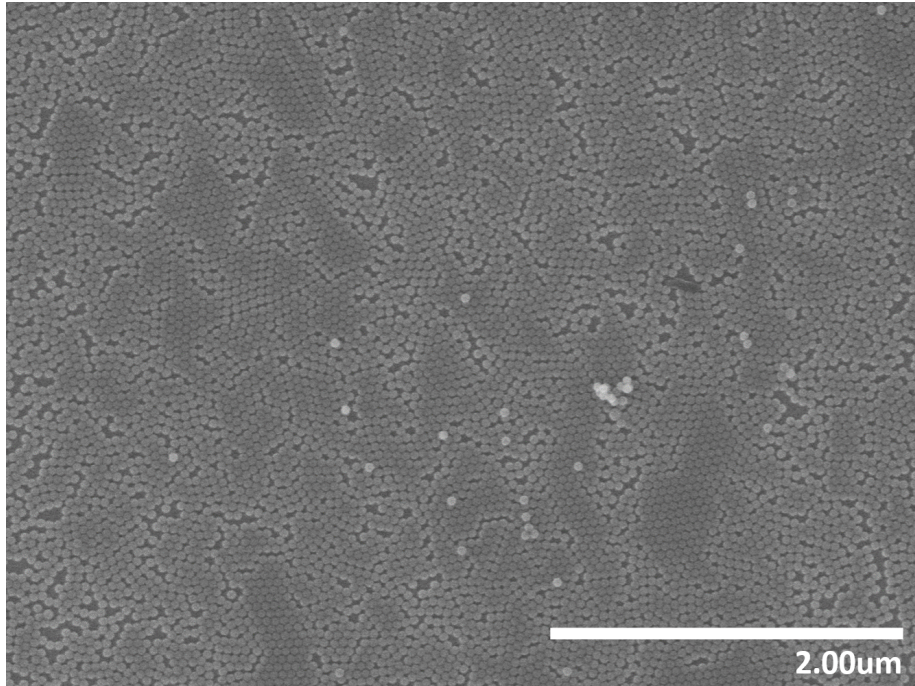


Figure 2: SEM image of a monolayer of SiO₂ NPs, assembled on a silicon wafer without extra toluene added after drop casting (without stearyl alcohol).

layer.

The fitting parameters obtained from the fitting of the x-ray reflectivity data of the monolayer film of nanoparticles after 10 days of heat treatment shown in Fig. 4 (c) in the main text are tabulated in table 2.

3.2 GISAXS

The intensity ratio for each GISAXS maps shown in Fig. 6 in the main text is quantified by comparing the integrated intensity of the Bragg rods to the integrated intensity of the diffuse rings. The intensity of the Bragg rods is integrated from $Q_z = 0.17 \text{ nm}^{-1} - 1.4 \text{ nm}^{-1}$, i.e. the area defined by the dotted orange rectangle in Fig. 3, while the intensity of the diffuse rings is performed from

Table 2: The parameters obtained from the fitting of the XRR data shown in Figure 4 (c) according to the model in Figure 4 (d).

Layer	Thickness (\AA)	Roughness (\AA)	$\rho(10^{-6}\text{\AA}^{-2})$
Silica layer	478(2)	5.2(5)	see text
Substrate	-	2.1(5)	21.6(1)

Table 3: The integrated intensity of the Bragg rods and the diffuse ring as calculated by integration over the areas defined by the dotted orange and white angle drawn in the GISAXS map in Fig. 3. The integrated intensity ratio between the GISAXS peaks and the diffuse rings from single defects are listed in column four.

Sample name	$I_{BR}[\text{arb. units}]$	$I_{DR}[\text{arb. units}]$	$\frac{I_{BR}}{I_{DR}}$
Without stearyl alcohol	7.2×10^{-3}	3×10^{-3}	2.4
With stearyl alcohol before heat treatment	1.4×10^{-2}	2×10^{-3}	7.5
With stearyl alcohol after 10 days of heat treatment	3.4×10^{-2}	6.8×10^{-6}	5130

$Q_z = -0.38 \text{ nm}^{-1} - 0.15 \text{ nm}^{-1}$, i.e. the area defined by the dashed white rectangle in Fig.3. The higher intensity ratio is found for the monolayer with stearyl alcohol after 10 days of heat treatment (methods 3).

The integrated intensity values of the Bragg rods and the diffuse rings of all GISAXS maps shown in Fig. 6 in the main text are listed in table 3. The integrated intensity as a function of Q_y of the Bragg rods and the diffuse rings of all GISAXS maps shown in Fig.6 (a-c) in the main text is shown in Fig.4 (a) and (b), respectively. The Bragg rods intensity of the sample after 10 days of heat treatment becomes higher (dark gray in Fig.4 (b)), while its diffuse rings intensity becomes less (dark gray in Fig.4 (a)). The high intensity ratio obtained for the sample after 10 days of heat treatment is an indication that most particles are taking part in the long-range order and scattering from individual defects is largely suppressed.

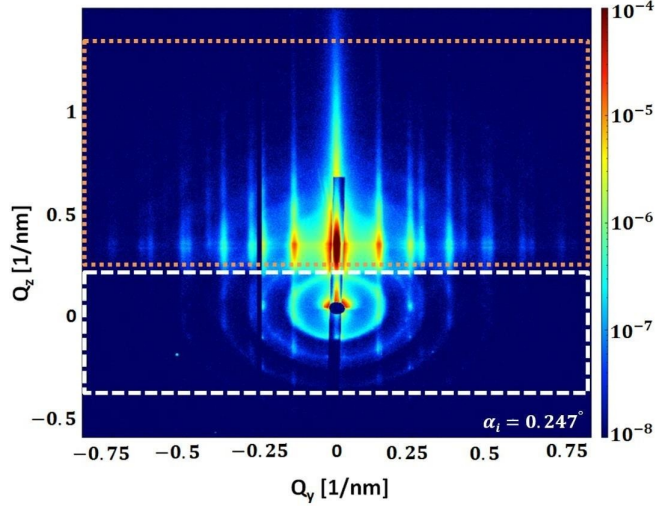


Figure 3: The 2D GISAXS map of the silica monolayer with stearyl alcohol after 10 days of heat treatment. The integrated intensity area of the Bragg rods is presented by a dotted orange rectangle and the integrated intensity area of the diffuse rings is presented by the white dashed rectangle.

3.3 Born Again Simulation

A Three-layer model is used to obtain the simulated pattern shown in Fig. 7 (b) in the main text. It consists of a silicon substrate followed by a natural silicon dioxide layer of 2 nm thickness on top of it and then the particles as a top layer. For both, Si and SiO₂ layers, natural roughness with an amplitude of 0.8 nm has been considered. Nanoparticles have a form factor of a full sphere with SiO₂ core of 23.5 nm radius and a stearyl alcohol shell of 1.7 nm thickness. The 3-D visualization of the model produced by the BornAgain software is shown in Fig. 5. Since nanoparticles are densely packed, the ambient layer, where the NPs are situated, has been described as a graded interface, i.e. it was sliced in 60 slices to account for the SLD gradient. As one can see from the SEM investigations (Figures. 1–3) in the main text, the sample is not uniformly covered with the NPs, but consists of ordered domains of variable size rotated with respect to each other. To account for this, finite 2D hexagonal lattices of randomly selected sizes have been simulated. To keep the simulation result reproducible, the random state has been fixed. Domain sizes

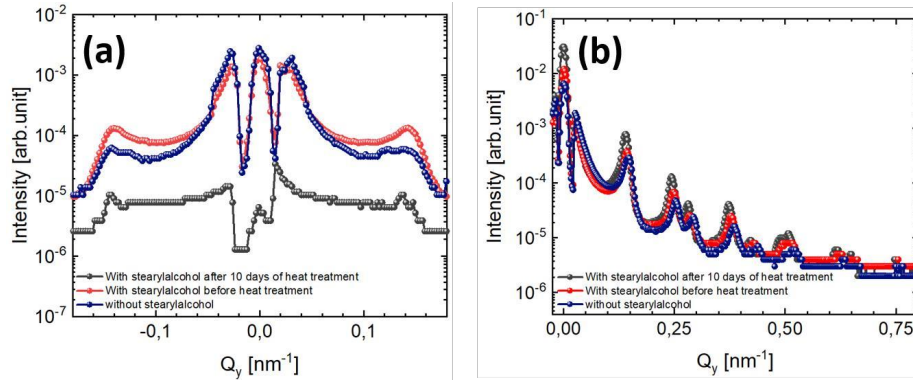


Figure 4: Integrated intensity of the (a) diffuse rings and (b) Bragg rods as a function of Q_y determined from the GISAXS maps shown in Fig. 6 (a-c) in the min text. The Bragg rods intensity is integrated from $Q_z = 0.17 \text{ nm}^{-1} - 1.4 \text{ nm}^{-1}$ and the diffuse rings intensity is integrated from $Q_z = -0.38 \text{ nm}^{-1} - 0.15 \text{ nm}^{-1}$.

were chosen from the uniform distribution. The lattice constant for all simulated lattices was kept a = 52 nm. To consider the polycrystallinity of the film, an orientational distribution has been applied to the simulated domains. Positions and relative intensities of the Bragg rods (Fig. 7(a) in the main text) indicate the absence of preferred domain orientations. Therefore, a uniform orientational distribution, i.e. 120 lattice rotation angles in the range between 0° and 60° with equal weights, has been simulated. The SAXS result presented in Fig. 1 shows that the nanoparticles have a size distribution. This contributes to diffuse scattering in the GISAXS pattern and broadens the structural peaks. To account for this effect, a Gaussian size distribution with FWHM of 3 nm has been applied in the GISAXS model.

As one can see from the results, the model reproduces the scattering from long-range order and even some disorder like particle size distribution or orientational distributions of the domains very well: the peak widths, relative intensities, and positions are the same for both, simulated and experimental GISAXS patterns. However, the simulated pattern has a valley in the region of small Q_z which is not seen in the experimental data as shown in Fig. 6. Moreover, simulated intensity decays with increasing Q_z noticeably faster than the measured one. These observations are signs of additional sample

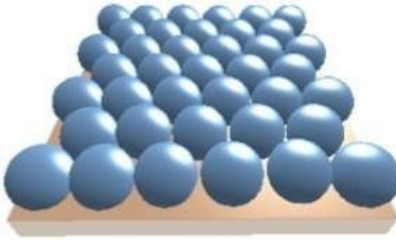


Figure 5: Three-dimensional vision of the simulated pattern shown in Figure 7 (b) in the main text.

features that are not considered by the present model and require further investigation in the future. Nevertheless, the present model provides a plausible characterization of SiO_2 NPs arrangements and allows for the determination of the film morphology, as is evident from the good match of experiment and simulation shown in Fig.7 (c) in the main text.

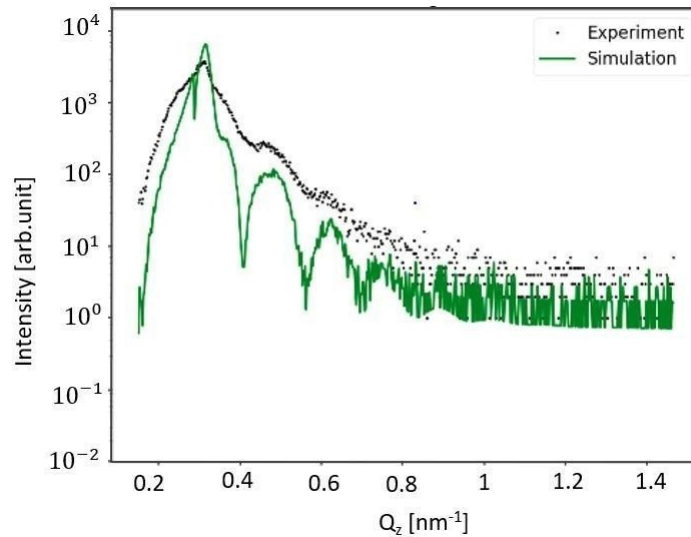


Figure 6: Slice along Q_Z at $Q_y = 0.14 \text{ nm}^{-1}$ (position of the first Bragg rod, shown with the vertical gray dashed line in Fig. 7 (a) and (b) in the main text).